arXiv:1804.04320v2 [astro-ph.CO] 4 Oct 2018

Falsifying ΛCDM: Model-independent tests of the concordance model with eBOSS DR14Q and Pantheon

Arman Shafieloo,[1,2,*] Benjamin L'Huillier,[1,†] and Alexei A. Starobinsky[3,4,‡]

[1] *Korea Astronomy and Space Science Institute, Yuseong-gu, Daedeok-daero 776, Daejeon 34055, Korea*
[2] *University of Science and Technology, Yuseong-gu 217 Gajeong-ro, Daejeon 34113, Korea*
[3] *L. D. Landau Institute for Theoretical Physics RAS, Moscow 119334, Russia*
[4] *National Research University Higher School of Economics, Moscow 101000, Russia*

We combine model-independent reconstructions of the expansion history from the latest Pantheon supernovae distance modulus compilation and measurements from baryon acoustic oscillation to test some important aspects of the concordance model of cosmology namely the FLRW metric and flatness of spatial curvature. We then use the reconstructed expansion histories to fit growth measurement from redshift-space distortion and obtain constraints on $(\Omega_{\rm m}, \gamma, \sigma_8)$ in a model independent manner. Our results show consistency with a spatially flat FLRW Universe with general relativity to govern the perturbation in the structure formation and the cosmological constant as dark energy. However, we can also see some hints of tension among different observations within the context of the concordance model related to high redshift observations ($z > 1$) of the expansion history. This supports earlier findings of [1, 2] and highlights the importance of precise measurement of expansion history and growth of structure at high redshifts.

I. INTRODUCTION

The concordance model of cosmology is based on Einstein's general theory of relativity (GR), which enabled us to build a theory of the Universe that is testable and can be falsified. The concordance flat ΛCDM model, which is based on GR and the assumptions of isotropy and homogeneity of the Universe, has been very successful at explaining various astronomical observations from a very early epoch (at least, from the Big-Bang nucleosynthesis time). This predictive model explains the dynamics of the Universe with only 6 free parameters. $\Omega_{\rm b}$ and $\Omega_{\rm dm}$ (baryonic and dark matter densities) are the matter parameters. Assuming a flat universe and cosmological constant being responsible for late time acceleration of the Universe, we can derive $\Omega_\Lambda = 1 - (\Omega_{\rm b} + \Omega_{\rm dm})$. τ representing the epoch of reionization, H_0 the Hubble parameter, n_s the spectral index of the primordial spectrum and A_s the overall amplitude of the primordial spectrum are the other 4 parameters of this model. Out of these parameters, the first four dictate the dynamic of the Universe and the other two represent the initial condition through the primordial fluctuations given by $P_R(k) = A_s \left(\frac{k}{k_*}\right)^{n_s - 1}$, where k_* is the pivot point. Having the form of the primordial fluctuations and the expansion history of the Universe one can determine the growth of structure for this model on linear scales following the linearised perturbation equation and also run N-body simulations to study the small scales and nonlinear regime. Despite the simplicity of the model, most astronomical observations are in great agreement with the concordance model and so far there has not been any strong observational evidence against it [e.g., 3–5]. In this paper we test some important aspects of the concordance model of cosmology in light of the most recent cosmological observations in a model-independent manner. At the background level, we derive the $H_0 r_d$ parameter, test dark energy as the cosmological constant Λ, the FLRW metric and the flatness of the Universe. At the perturbation level, we then use model independent reconstruction of the expansion history from supernovae data to fit growth of structure data and put model independent constraints on some key cosmological parameters, namely $\Omega_{\rm m}, \gamma$, and σ_8. In § II we describe the background expansion and our tests on Λ dark energy, FLRW metric and flatness of the spatial curvature. Analysis on the growth of structure and testing general theory of relativity are presented in § III, and our conclusions are drawn in § IV.

II. BACKGROUND EXPANSION: TESTING Λ, THE FLRW METRIC, AND THE CURVATURE

At the background level, it is possible to test dark energy as Λ, the FLRW metric, and the curvature of the Universe. In a FLRW universe with a dark energy component of equation of state $w(z)$, the luminosity distance can be written for any curvature Ω_k

$$d_{\rm L}(z) = \frac{c}{H_0}(1+z)\mathcal{D}(z), \tag{1}$$

where

$$\mathcal{D}(z) = \frac{1}{\sqrt{-\Omega_k}} \sin\left(\sqrt{-\Omega_k}\int_0^z \frac{{\rm d}x}{h(x)}\right) \tag{2}$$

* shafieloo@kasi.re.kr
† benjamin@kasi.re.kr
‡ alstar@landau.ac.ru

is the dimensionless comoving distance, and

$$h^2(z) = \left(\frac{H(z)}{H_0}\right)^2 = \Omega_{\rm m}(1+z)^3 + \Omega_k(1+z)^2 + (1-\Omega_{\rm m}-\Omega_k)\exp\left(3\int_0^z \frac{1+w(x)}{1+x}{\rm d}x\right) \quad (3)$$

is the expansion history. Having different observables of the cosmic distances and expansion history one can then introduce novel approaches to examine the FLRW metric, flatness of the Universe and Λ dark energy in a model-dependent [e.g., 6] or independent way [2, 7–12]. Note that one can also test the metric and the curvature using gravitational lensing [e.g. 13, 14] or cosmic parallaxes [15].

A. Model-independent reconstruction of the expansion history from the Pantheon compilation

In order to reconstruct the $D(z)$, $D'(z)$ and $h(z)$ at any given redshift, we apply the iterative smoothing method [10, 16–18] to the the latest compilation of supernovae distance modulus [Pantheon, 5]. Pantheon is the latest compilation of 1048 SNIa, extending previous compilations with confirmed SNIa from the Pan-STARRS1 survey.

The method of smoothing is a fully model independent approach to reconstruct the $D(z)$ relation directly from the supernova data, without assuming any particular model or a parametric form. The only parameter used in the smoothing method is the smoothing width Δ, which is constrained only by the quality and quantity of the data. The smoothing method is an iterative procedure with each iteration providing a better fit to the data. It has been discussed and shown that the final reconstructed results are independent of the assumed initial guess [16–18]. In our analysis we start the smoothing procedure from various arbitrary choices of the initial guess models and while their final results converge to the same reconstruction, we select within the process, a non-exhaustive samples of the reconstructions that have a χ^2 better than the best fit ΛCDM model. In [18] the method of smoothing was modified to incorporate the data uncertainties and hence making the approach error-sensitive. However, the formalism in [18] could take in to account only the diagonal terms of the error matrix. While the quality of the data is improving continuously and non-diagonal terms of the covariance matrices can play an important role in likelihood estimations, in this work we modify the smoothing method further by incorporating the whole covariance matrix of the data in to the smoothing procedure. While this improvement might look like a minor modification, it is in fact a very important step to make this model independent reconstruction approach complete and comprehensive to deal with highly correlated data.

In order to take into account the non-diagonal terms of the covariance matrix, we modified the method in the following way. Starting with some initial guess $\hat{\mu}_0$, we iteratively calculate the reconstructed $\hat{\mu}_{n+1}$ at iteration $n+1$:

$$\hat{\mu}_{n+1}(z) = \hat{\mu}_n(z) + \frac{\boldsymbol{\delta\mu}_n^{\rm T}\cdot\mathbf{C}_{\rm SN}^{-1}\cdot\boldsymbol{W}(z)}{\mathbb{1}^T\cdot\mathbf{C}_{\rm SN}^{-1}\cdot\boldsymbol{W}(z)}, \quad (4)$$

where the weight $\boldsymbol{W}$ and residual $\boldsymbol{\delta\mu_n}$ are defined as

$$\boldsymbol{W}_i(z) = \exp\left(-\frac{\ln^2\left(\frac{1+z}{1+z_i}\right)}{2\Delta^2}\right) \quad (5)$$

$$\boldsymbol{\delta\mu}_n|_i = \mu_i - \hat{\mu}_n(z_i), \quad (6)$$

$$\mathbb{1}^T = (1,\ldots,1), \quad (7)$$

and $\mathbf{C}_{\rm SN}$ is the covariance matrix of the data (in our case, Pantheon data). In case of uncorrelated data ($C_{ij} = \delta_{ij}\sigma_i^2$)), we recover the formula introduced in [18] used recently in [10].

The χ^2 of the reconstruction $\hat{\mu}_n(z)$ is then defined as

$$\chi^2_n = \boldsymbol{\delta\mu}_n^{\rm T}\cdot\mathbf{C}_{\rm SN}^{-1}\cdot\boldsymbol{\delta\mu}_n, \quad (8)$$

and in this work we only consider reconstructions with $\chi^2 < \chi^2_{\Lambda{\rm CDM\ best\text{-}fit}}$.

The result of the smoothing procedure is thus $H_0\hat{d}_{{\rm L}n}(z) = 10^{(\hat{\mu}_n-5)/5}$. Under the assumption of a flat Universe, we can obtain $h_n(z) = 1/({\rm d}\mathcal{D}_n(z)/{\rm d}z)$.

We should clarify here that our selected reconstructions of the expansion history from the iterative smoothing method are not posterior samples within a Bayesian framework. We in fact obtain a non-exhaustive sample of plausible expansion histories, directly reconstructed by supernova data and with no model assumption, which all give a better χ^2 to the Pantheon data than the best-fit ΛCDM model. This enables us to explore regions of the physical space of the expansion history beyond the flexibility of the concordance model (or other parametric functional forms) that can fit the data reasonably well. Note that the formalism given in this paper for the method of smoothing is self-contained and has all needed information. Equations (4) to (8) contain the full formalism of the iterative smoothing method including the full covariance matrix of the data, which is now simply written in a matricial way (which is more compact). However, for more details and better understanding of the method one can follow the given references.

B. BAO measurements of cosmic distances and expansion history

The radial mode of the BAO measures $H(z)r_{\rm d}$, while the transverse modes provide $d_{\rm A}(z)/r_{\rm d}$, where

$$r_{\rm d} = \frac{c}{\sqrt{3}} \int_0^{1/(1+z_{\rm drag})} \frac{{\rm d}a}{a^2 H(a) \sqrt{1 + \frac{3\Omega_{\rm b}}{4\Omega_{\rm r}} a}} \qquad (9)$$

is the sound horizon at the drag epoch $z_{\rm drag}$. We combined the Baryon Oscillation Spectroscopic Survey (BOSS) DR12 consensus values [4] and the extended-BOSS (eBOSS) DR14Q measurements [19]. We note that both BOSS DR12 and eBOSS DR14Q provide $H(z)r_{\rm d}/r_{\rm d,fid}$ and $d_{\rm A}(z)r_{\rm d,fid}/r_{\rm d}$ with $r_{\rm d,fid} = 147.78\,{\rm Mpc}$. We also include the Dark Energy Survey DR1 (DES DR1) measurement of $d_{\rm A}/r_{\rm d}$ at $z = 0.81$ [20]. We use these BAO data along with our reconstructions of the expansion history from supernova data as two independent sets of observations to test some key aspects of the concordance model.

C. Testing Λ Dark Energy

The solid black lines in Fig. 1 show the different reconstructed $\mathcal{D}(z)$, $h(z) = 1/\mathcal{D}'(z)$ and $Om(z)$ from Pantheon supernovae compilation where $Om(z)$ is defined as [8]:

$$Om(z) = \frac{h^2 - 1}{(1+z)^3 - 1} \qquad (10)$$

We also show in Fig. 1 the BAO data points for these quantities. Since the BAO measure $H(z)r_{\rm d}$ and $d_{\rm A}(z)/r_{\rm d}$, to have a good sense of comparison within the context of the concordance model, we normalize them by $H_0 r_{\rm d}$ from Planck 2015 (TTTEEE+LowP+Lensing) best fit ΛCDM model, and show on the top panel $\mathcal{D}(z) = (1+z)H_0 r_{\rm d} d_{\rm A}(z)/(c r_{\rm d})$, in the middle panel $h(z) = H(z)r_{\rm d}/H_0 r_{\rm d}$ and the corresponding $Om(z)$ on the bottom panel. The magenta solid line shows the corresponding $\mathcal{D}(z)$, $h(z)$ and $Om(z)$ for the best-fit Planck 2015 Flat-ΛCDM model.

While the reconstructed expansion history $h(z)$ from SNIa are fully consistent with the BAO data points at low redshifts ($z \leq 1.2$), some tension seems to arise at higher redshifts ($z \geq 1.5$) where the reconstructed expansion histories from the BAO data suggest lower $h(z)$ with respect to the best fit ΛCDM model from Planck. While the errorbars are still quite large, the BAO data seem to follow the same trend in suggesting lower values of $h(z)$ (with respect to the best fit ΛCDM model from Planck) at high redshifts. For illustration purpose we also show the measurement of $h(z = 2.33)$ from the Lyman-α forest [21] which seems to agree with other BAO data points suggesting lower $h(z)$ with respect to Planck best fit ΛCDM model, although we did not include this data point in our analysis since the supernovae data do not reach such a high redshift. This data point is consistent with the previous result from SDSS III [22]. This tension is also visible clearly looking at the Om diagnostic in bottom plot of Fig. 1, which is also consistent with the finding of [1]. If dark energy is a cosmological constant (and if the Universe is flat), the Om diagnostic should be constant in redshift. Therefore, having different values from different observations suggests some tension among the data within the framework of the concordance model.

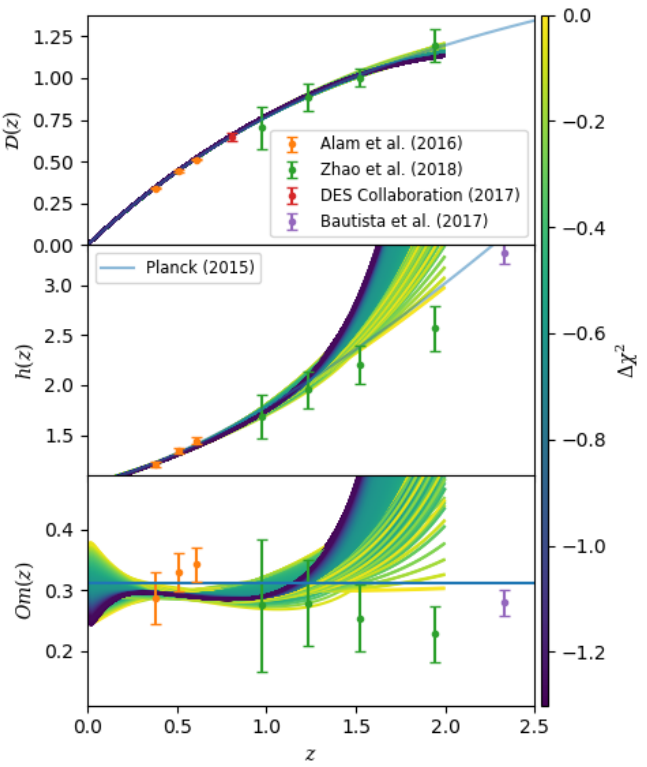


FIG. 1: BAO data points normalized by $H_0 r_{\rm d}$ from [3] best fit ΛCDM model. The solid lines are the reconstructed expansion histories from the Pantheon data which are fully model independent, and the purple line is the prediction from [3] for the best-fit concordance ΛCDM model. They are color-coded by their $\Delta\chi^2$ with respect to the best-fit ΛCDM model, with earlier iterations having less negative $\delta\chi^2$ (yellow), and later iterations more negative $\Delta\chi^2$ (dark blue).

Meanwhile, the comoving distances $\mathcal{D}(z)$ from BAO and SNIa are fully consistent together and with the best-fit Planck cosmology. Combining these results of the comoving distances and expansion histories may show some inconsistency with flatness as we will see later in this work.

D. Estimating $H_0 r_{\rm d}$

Ref. [10] estimated $H_0 r_{\rm d}$ in a model-independent way by combining BAO measurements and reconstructions of

the expansion history from supernovae. $H_0 r_\mathrm{d}$ is an important parameter combining physics of the early (sound horizon at the drag epoch) and late Universe (expansion rate). For each reconstruction n, we can calculate $H_0 r_\mathrm{d}$ in two different ways

$$H_0 r_\mathrm{d}|_{d_\mathrm{A},n} = \frac{c}{1+z}\mathcal{D}_n(z)\frac{r_\mathrm{d}}{d_\mathrm{A}(z)} \tag{11a}$$

$$H_0 r_\mathrm{d}|_{H,n} = \frac{H(z) r_\mathrm{d}}{h_n(z)}, \tag{11b}$$

and their associated errors

$$\sigma_{H_0 r_\mathrm{d}}|_{d_\mathrm{A},n} = \frac{c}{1+z}\mathcal{D}_n(z)\frac{\sigma_{d_\mathrm{A}/r_\mathrm{d}}(z)}{(d_\mathrm{A}(z)/r_\mathrm{d})^2} \tag{12a}$$

$$\sigma_{H_0 r_\mathrm{d}}|_{H,n} = \frac{\sigma_{H r_\mathrm{d}}(z)}{h_n(z)}, \tag{12b}$$

where, assuming a flat-FLRW universe, $h(z) = 1/\mathcal{D}'(z)$.

Fig. 2 shows our estimation of $H_0 r_\mathrm{d}$ at the different BAO data points for the two estimations. In green is shown the ΛCDM value from Planck 2015 [3]. We can then define two error-bars. The first one is the error due to the supernova. At fixed redshift, we define $\langle H_0 r_\mathrm{d}\rangle_X$ as the median over all reconstructions for method $X \in \{d_\mathrm{A}, H\}$. We can then define the upper and lower limit as the minimal and maximal values of $H_0 r_\mathrm{d}|_{X,n}$. This error-bar is shown as a dashed line in Fig. 2. The second error is due to the uncertainty on the BAO (equations (12a) and (12b)), and is the uncertainty of the central value for a given reconstruction n. For each reconstruction n and method X, we have an error $\sigma_{H_0 r_\mathrm{d}}|_{X,n}$. They are of the same order for each reconstruction, so we define the final BAO error as the maximum value over all reconstructions. This error-bar is shown as a solid error-bar in Fig. 2.

For the first method (in orange), the measurements of $H_0 r_\mathrm{d}$ from combination of supernova and SDSS BAO data are fully consistent with Planck. The DES data point, also using the transverse BAO mode, is an independent confirmation at intermediate redshift. However, for the second method, while at low redshift, the measurements are consistent with Planck, the eBOSS data points are systematically lower than the Planck best-fit at $z \geq 1.2$ while the errorbars become very large at this range. This can be understood by the following remarks.

The first method yields very consistent results thanks to the use of the transverse BAO mode, which has smaller error-bars, coupled with direct reconstructions $\mathcal{D}(z)$ which do not use derivative.

The second method however, uses the line-of-sight mode of the BAO, together with $h(z)$ from supernovae data which is a derivative. Since the Pantheon data become scarce at $z \geq 1$, the estimation of $h(z)$ becomes less precise at this range having large error-bars. Combination of these two results to large uncertainties for $H_0 r_\mathrm{d}$ from the second method. On the other hand, it can be seen from Fig. 1 that while $h(z)$ from SNIa are higher than the best-fit Planck ΛCDM model, $h(z)$ from the BAO (scaled with best fit Planck ΛCDM model) are actually lower. This explains the lower values of $H(z)r_\mathrm{d}/h(z)$ at the eBOSS redshifts with respect to the other measurements.

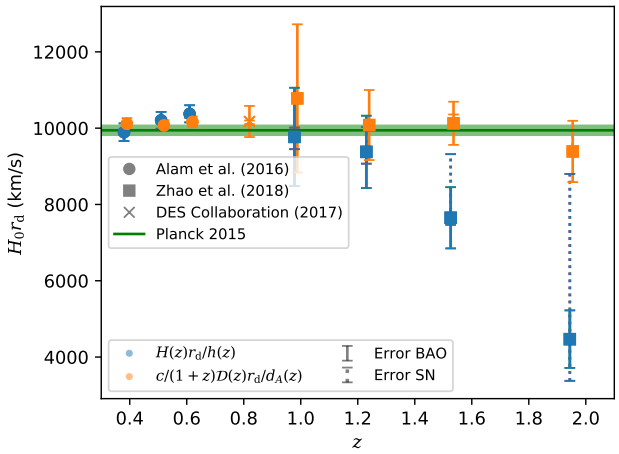


FIG. 2: Model-independent measurement of $H_0 r_\mathrm{d}$ estimated at the different BAO data points. The dotted error-bars show the range of possible central values from different reconstructions (SN error), while the solid error bars show the uncertainty on the central value (BAO error).

We can then estimate, for each reconstruction n and method $X \in \{d_\mathrm{A}, H\}$, the weighted average

$$\langle H_0 r_\mathrm{d}\rangle_{X,n} = \frac{\mathbb{1}^T \cdot \mathbf{C}_n^{-1} \cdot \boldsymbol{H_0 r}_\mathrm{d}|_{X,n}}{\mathbb{1}^T \cdot \mathbf{C}_n^{-1} \cdot \mathbb{1}}, \tag{13}$$

where $\boldsymbol{H_0 r}_\mathrm{d}|_{X,n}$ is a vector constituted of estimations of $H_0 r_\mathrm{d}$ at different redshifts for iteration n, and $\mathbf{C}_n$ is the associated covariance matrix (due to the correlation in the BAO data). We report our results in Table I. The Planck 2015 value of $H_0 r_\mathrm{d}$ for the ΛCDM model is $(9944.0 \pm 127.4)\,\mathrm{km\,s^{-1}\,Mpc^{-1}}$. We should note an important interpretation of this result. While all our reconstructions of the expansion history from supernovae data have better χ^2 with respect to the best fit ΛCDM model, our large uncertainties on $H_0 r_\mathrm{d}$ indicates that tight constraints on this quantity from model dependent approaches (such as assuming ΛCDM model) have limitations in expressing the reality of the universe and estimating its key parameters.

E. Test of the FLRW metric and the curvature

[10] reformulated the $\mathcal{O}_k$ diagnostic [7] by introducing the Θ diagnostic so that it now only depends on the BAO

TABLE I: Weighted average of $H_0 r_\mathrm{d}$ from the H and d_A methods.

Method	$H_0 r_\mathrm{d}$	Error SN	Error BAO
$\langle H_0 r_\mathrm{d}\rangle_{d_\mathrm{A}}$ (km s^{-1})	10120.42	$^{+33.79}_{-59.12}$	$\pm$103.92
$\langle H_0 r_\mathrm{d}\rangle_{H}$ (km s^{-1})	9162.80	$^{+875.06}_{-921.02}$	$\pm$166.39

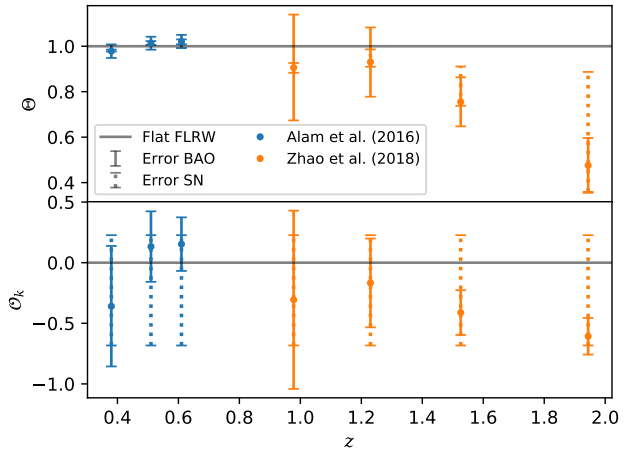


FIG. 3: FLRW and curvature test: $\Theta(z)$ (top) and $\mathcal{O}_k(z)$ (bottom). The dotted error-bars show the range of possible central values from different reconstructions (SN error), while the solid error bars show the uncertainty on the central value (BAO error). For a flat-FLRW Universe, $\Theta(z) \equiv 1$ and $\mathcal{O}_k(z) \equiv \Omega_k$.

and supernovae observables:

$$\mathcal{O}_k(z) = \frac{\Theta^2(z) - 1}{\mathcal{D}^2(z)} \tag{14a}$$

$$\Theta(z) = h(z)\mathcal{D}'(z) = \frac{1+z}{c} H(z) r_\mathrm{d} \frac{d_\mathrm{A}(z)}{r_\mathrm{d}} \frac{\mathcal{D}'(z)}{\mathcal{D}(z)}. \tag{14b}$$

For a FLRW Universe, $\mathcal{O}_k(z) \equiv \Omega_k$, and in case of flatness, $\mathcal{O}_k(z) \equiv 0$ and $\Theta(z) \equiv 1$. We can then calculate for each reconstruction n the associated $\mathcal{O}_{k,n}(z)$ and $\Theta_n(z)$. We calculated the median of $\mathcal{O}_k$ and Θ over all reconstructions, and defined the SN error as the minimal and maximal values, and the BAO error as the maximal error over all reconstructions. Fig. 3 shows $\Theta(z)$ (top) and $\mathcal{O}_k(z)$ (bottom). Both are consistent with a flat FLRW metric up to $z \simeq 1.2$.

However, at high redshift, some deviation from flatness can be seen. Again, this can be explained by the previous remarks. In addition to the scarcity of the SN data at $z \geq 1.5$, which results in into poor constraints on $h(z)$, the BAO seem to show some internal tensions. While $d_\mathrm{A}(z)/r_\mathrm{d}$ are consistent with the Planck best-fit, $H(z) r_\mathrm{d}$ are lower than expected. However, the Θ and $\mathcal{O}_k$ statistics assume a FLRW metric, where d_A and H are related to each other. Thus, discrepancy between d_A and H combined with the higher h values at high-redshift ($z \geq 1$) yields lower values for Θ and $\mathcal{O}_k$. We should also note that in the case of supernova data, the Malmquist bias (if not treated carefully) can pull down the $\mathcal{D}(z)$ relation at high redshifts. This might explain the large swing upward of $h(z)$ and $Om(z)$ (with respect to the best-fit ΛCDM case) that we can see in Fig. 1, and consequently the apparent deviation from flatness observed in Θ and $\mathcal{O}_k$. While it is certainly important to study further this effect in the case of the Pantheon data, it is beyond the scope of this paper.

III. GROWTH OF STRUCTURE VERSUS EXPANSION: TESTING GR

At the perturbation level, the cosmological growth of structure can also serve as a test of gravity [11, 23–34]. In the linear regime, the growth of structure in GR follows

$$\ddot{\delta} + 2H\dot{\delta} - 4\pi G\bar{\rho}\delta = 0, \tag{15}$$

where $\delta = \rho/\bar{\rho} - 1$ is the density contrast with respect to the mean density of the Universe $\bar{\rho}$. The growth rate

$$f(a) = \frac{\mathrm{d}\ln\delta}{\mathrm{d}\ln a} \tag{16}$$

can be approximated for a wide range of cosmologies by [35–37]

$$f(z) = \Omega_\mathrm{m}^\gamma(z), \tag{17}$$

where

$$\Omega_\mathrm{m}(z) = \frac{\Omega_\mathrm{m}(1+z)^3}{h^2(z)}. \tag{18}$$

In general relativity (GR), $\gamma \simeq 0.55$. $f\sigma_8$ is thus a powerful probe of gravity. Observationally, redshift-space distortion enables to measure the combination [e.g. 24]

$$f\sigma_8(z) \simeq \sigma_8 \Omega_\mathrm{m}^\gamma(z) \exp\left(-\int_0^z \Omega_\mathrm{m}^\gamma(x) \frac{\mathrm{d}x}{1+x}\right), \tag{19}$$

where $\sigma_8 = \sigma_8(z=0)$ is the rms fluctuation in $8\,h^{-1}$Mpc spheres. Following this formalism, having model independent reconstructions of the expansion history and $f\sigma_8(z)$ data, one can obtain constraints on Ω_m,γ, and σ_8 [38]. Note that we consider the estimated $f\sigma_8$ data from BAO surveys as an independent and uncorrelated measurements with respect to the supernova data that we used to reconstruct the expansion history.

Note, however, that one should keep in mind that Eq. (17) is an approximate fit only. In particular, γ may not be exactly constant for quintessence—dark energy modelled by a scalar field with some potential minimally coupled to gravity [39]. Still both for ΛCDM and for quintessence-CDM this fit is good since $\frac{\mathrm{d}\gamma}{\mathrm{d}z}$ is small as far as Ω_m is not too small, see also [40]. For modified gravity theories like $f(R)$ gravity, the situation can be different [41, 42].

A. Cosmological constraints on $\Omega_{\rm m}, \gamma, \sigma_8$

Following [38], we combined the Pantheon compilation with the latest measurements of $f\sigma_8$: 2dFGRS [24], WiggleZ [43], 6dFGRS [44], VIPERS [45], the SDSS Main galaxy sample [46], 2MTF [47], BOSS DR12 [48], FastSound [49], and eBOSS DR14Q [19]. In this section, we assume a flat Universe, therefore

$$h(z) = \frac{1}{\mathcal{D}'(z)}. \tag{20}$$

It is worth noting that these measurements, coming from different surveys, were obtained assuming different fiducial cosmologies. Therefore, we correct for the fiducial cosmology [32, 50]. The growth χ^2 for the nth reconstruction $h_n(z)$ and parameters $\boldsymbol{p} = (\Omega_{\rm m}, \gamma, \sigma_8)$ is thus given by

$$\chi^2_{n,f\sigma_8}(\boldsymbol{p}) = \boldsymbol{\delta f\sigma_{8n}} \cdot \mathbf{C}^{-1}_{f\sigma_8} \cdot \boldsymbol{\delta f\sigma_{8n}}, \tag{21}$$

where $\mathbf{C}_{f\sigma_8}$ is the growth covariance matrix, and the ith component of the residual vector $\boldsymbol{\delta f\sigma_{8}}_n$ is

$$\delta f\sigma_{8n}|_i = \frac{h_n(z_i)\mathcal{D}_n(z_i)}{(1+z_i)H_{\rm fid}(z_i)d_{\rm A,fid}(z_i)}\widehat{f\sigma_8}_n(z_i|\boldsymbol{p}, h_n) - f\sigma_8|_i. \tag{22}$$

The total χ^2 for reconstruction n and parameter $\boldsymbol{p}$ is then

$$\chi^2_{n,\rm tot}(\boldsymbol{p}) = \chi^2_{n,f\sigma_8}(\boldsymbol{p}) + \chi^2_{n,\rm SN}, \tag{23}$$

where $\widehat{f\sigma_8}(z_i|\boldsymbol{p}, h_n)$ is the model corresponding to the expansion history h_n and parameters $\boldsymbol{p}$ and fid stands for the fiducial cosmology used by the survey to estimate the data point.

The red contours in the $(\sigma_8, \Omega_{\rm m})$ plane in Fig. 4 show the 1σ and 2σ regions of the parameter space in the flat ΛCDM case, that is, flat-ΛCDM expansion history and $\gamma = 0.55$. The blue contours show the allowed parameter space in the model-independent case. Namely, for any point in the blue contours, one can find at least one reconstruction $h(z)$ which, combined to the corresponding $(\Omega_{\rm m}, \gamma, \sigma_8)$, gives a better fit to the data than the best-fit ΛCDM. In the $(\sigma_8, \Omega_{\rm m})$ plane, the model-independent case is fully consistent with the ΛCDM case. Moreover, the flexibility of the model-independent approach allows a larger area of the parameter space to be consistent to the data. For instance, for larger values of σ_8 and lower values of $\Omega_{\rm m}$, one can find reconstructed expansion histories that give a better total fit to the data (SNIa+growth) with respect to the best fit ΛCDM model. For the model-independent case, γ is fully consistent with 0.55, as expected from GR. Moreover, lower value of γ, combined with lower value of $\Omega_{\rm m}$ and larger σ_8, can also provide good fit to the data.

We then fix $\gamma = 0.55$, as we did for the ΛCDM case, and show in Fig. 4 the corresponding confidence contours

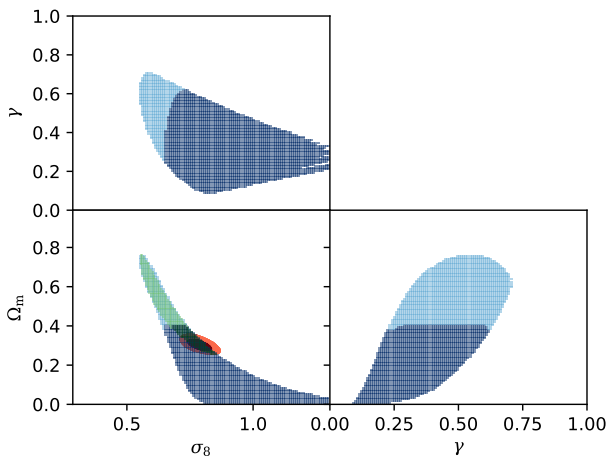


FIG. 4: Model independent cosmological constraints on $(\Omega_{\rm m}, \gamma, \sigma_8)$ from growth and expansion data. The red contours are the 1σ and 2σ confidence levels for the ΛCDM case. The blue contours are associated to the combination of the parameters and reconstructions of the expansion history that yield a better χ^2 with respect to the best-fit ΛCDM model. The dark-blue region satisfy positive dark energy density condition as expressed in equation (24). The green contours show the model-independent case where we fixed $\gamma = 0.55$, i.e., impose GR. Again, the dark contours satisfy equation (24).

in green. This effectively allows for a non-ΛCDM background expansion, with gravity as GR. This time, since we do not allow γ to vary, the region with low $\Omega_{\rm m}$ and high σ_8 is now forbidden.

Finally, following [38], we focus on combinations of $h(z)$ and $\Omega_{\rm m}$ that respect the positive dark energy condition

$$\Omega_{\rm de}(z) = h^2(z) - \Omega_{\rm m}(1+z)^3 \geq 0 \qquad \forall z. \tag{24}$$

We show this region in dark-blue (free γ) and dark-green (fixed γ) in Fig. 4. Imposing equation (24) effectively forbids large values of $\Omega_{\rm m}$, and dramatically reduces the allowed parameter space of the model-independent case. The allowed region of the parameter space is then fully consistent with the model-dependent case, as in [38]. This is a strong support from the data for combination of ΛCDM and GR. Comparing our results here using most recent supernovae (Pantheon compilation) and BAO data (from eBOSS DR14) with what was reported in [38] we can notice substantial improvement on the constraints on these three key cosmological parameters. Based on our analysis we can now put strong model-independent upper bound limits on $\Omega_{\rm m} < 0.42$ and $\gamma < 0.58$ and a lower bound limit on $\sigma_8 > 0.70$. These are in fact model independent constraints on these key cosmological parameters.

IV. SUMMARY AND CONCLUSIONS

We used the Pantheon supernovae compilation to reconstruct the expansion history in a model-independent way, using an improved version of the iterative smoothing method [10, 16–18], which we modified to take into account the non-diagonal terms of the full covariance matrix. We then combined the reconstructed expansion histories to measurements of $H(z)r_{\rm d}$ and $d_{\rm A}(z)/r_{\rm d}$ from BOSS DR12 and eBOSS DR14Q to model-independently measure $H_0 r_{\rm d}$ and test the FLRW metric. Our measurements of $H_0 r_{\rm d}$ are consistent with the Planck 2015 values, while the metric test is consistent with a Flat-FLRW metric. However, for the eBOSS DR14Q data points, while $d_{\rm A}(z)/r_{\rm d}$ is consistent with the prediction from the Planck best-fit ΛCDM cosmology, the $H(z)r_{\rm d}$ measurements are slightly but systematically lower. This yields some hints for a departure from flat-FLRW (Fig. 3) and supports previous findings of [1] & [2].

We then fit the growth data from redshift space distortion, mainly from SDSS survey using the model-independent reconstructions of the expansion history, and put model-independent constraints on $\Omega_{\rm m} < 0.42$, $\gamma < 0.58$ and $\sigma_8 > 0.70$. Our measurements are fully consistent with the ΛCDM model with GR ($\gamma \approx 0.55$), and do not reveal any tension between the two data sets.

Future surveys, such as the Dark Energy Spectroscopic Instrument [51, 52], the Large Synoptic Telescope [53], and WFIRST, will improve the quality and quantity of data, enabling us to detect any possible deviation from ΛCDM.

ACKNOWLEDGEMENTS

We thank Gongbo Zhao and Yuting Wang for useful discussions, and Dan Scolnic for providing the Pantheon data. This work benefited from the Supercomputing Center/Korea Institute of Science and Technology Information with supercomputing resources including technical support (KSC-2016-C2-0035 and KSC-2017-C2-0021) and the high performance computing clusters Polaris and Seondeok at the Korea Astronomy and Space Science Institute. A.S. would like to acknowledge the support of the National Research Foundation of Korea (NRF-2016R1C1B2016478). A. A. S. was partly supported by the program P-28 "Cosmos" of the Russian Academy of Sciences (the project number 0033-2018-0013 of the Federal Agency of Scientific Organizations of Russia).

[1] V. Sahni, A. Shafieloo, and A. A. Starobinsky, ApJ **793**, L40 (2014), 1406.2209.
[2] G.-B. Zhao, M. Raveri, L. Pogosian, Y. Wang, R. G. Crittenden, W. J. Handley, W. J. Percival, F. Beutler, J. Brinkmann, C.-H. Chuang, et al., Nature Astronomy **1**, 627 (2017), 1701.08165.
[3] Planck Collaboration XIII, A&A **594**, A13 (2016), 1502.01589.
[4] S. Alam, M. Ata, S. Bailey, F. Beutler, D. Bizyaev, J. A. Blazek, A. S. Bolton, J. R. Brownstein, A. Burden, C.-H. Chuang, et al., MNRAS **470**, 2617 (2017), 1607.03155.
[5] D. M. Scolnic, D. O. Jones, A. Rest, Y. C. Pan, R. Chornock, R. J. Foley, M. E. Huber, R. Kessler, G. Narayan, A. G. Riess, et al., ApJ **859**, 101 (2018), 1710.00845.
[6] O. Farooq and B. Ratra, Physics Letters B **723**, 1 (2013), 1212.4264.
[7] C. Clarkson, B. Bassett, and T. H.-C. Lu, Physical Review Letters **101**, 011301 (2008), 0712.3457.
[8] V. Sahni, A. Shafieloo, and A. A. Starobinsky, Phys. Rev. D **78**, 103502 (2008), 0807.3548.
[9] D. Sapone, E. Majerotto, and S. Nesseris, Phys. Rev. D **90**, 023012 (2014), 1402.2236.
[10] B. L'Huillier and A. Shafieloo, J. Cosmology Astropart. Phys. **1**, 015 (2017), 1606.06832.
[11] V. Marra and D. Sapone, Phys. Rev. D **97**, 083510 (2018), 1712.09676.
[12] F. Montanari and S. Räsänen, J. Cosmology Astropart. Phys. **11**, 032 (2017), 1709.06022.
[13] S. Räsänen, K. Bolejko, and A. Finoguenov, Physical Review Letters **115**, 101301 (2015), 1412.4976.
[14] M. Denissenya, E. V. Linder, and A. Shafieloo, J. Cosmology Astropart. Phys. **3**, 041 (2018), 1802.04816.
[15] S. Räsänen, J. Cosmology Astropart. Phys. **3**, 035 (2014), 1312.5738.
[16] A. Shafieloo, U. Alam, V. Sahni, and A. A. Starobinsky, MNRAS **366**, 1081 (2006), astro-ph/0505329.
[17] A. Shafieloo, MNRAS **380**, 1573 (2007), astro-ph/0703034.
[18] A. Shafieloo and C. Clarkson, Phys. Rev. D **81**, 083537 (2010), 0911.4858.
[19] G.-B. Zhao, Y. Wang, S. Saito, H. Gil-Marín, W. J. Percival, D. Wang, C.-H. Chuang, R. Ruggeri, E.-M. Mueller, F. Zhu, et al., ArXiv e-prints (2018), 1801.03043.
[20] The Dark Energy Survey Collaboration, T. M. C. Abbott, F. B. Abdalla, A. Alarcon, S. Allam, F. Andrade-Oliveira, J. Annis, S. Avila, M. Banerji, N. Banik, et al., ArXiv e-prints (2017), 1712.06209.
[21] J. E. Bautista, N. G. Busca, J. Guy, J. Rich, M. Blomqvist, H. du Mas des Bourboux, M. M. Pieri, A. Font-Ribera, S. Bailey, T. Delubac, et al., A&A **603**, A12 (2017), 1702.00176.
[22] T. Delubac, J. E. Bautista, N. G. Busca, J. Rich, D. Kirkby, S. Bailey, A. Font-Ribera, A. Slosar, K.-G. Lee, M. M. Pieri, et al., A&A **574**, A59 (2015), 1404.1801.
[23] S. Nesseris and L. Perivolaropoulos, Phys. Rev. D **77**, 023504 (2008), 0710.1092.
[24] Y.-S. Song and W. J. Percival, J. Cosmology Astropart. Phys. **10**, 004 (2009), 0807.0810.
[25] V. Acquaviva and E. Gawiser, Phys. Rev. D **82**, 082001 (2010), 1008.3392.

[26] S. Basilakos, International Journal of Modern Physics D **21**, 1250064 (2012), 1202.1637.

[27] A. Shafieloo, A. G. Kim, and E. V. Linder, Phys. Rev. D **87**, 023520 (2013), 1211.6128.

[28] A. Pavlov, O. Farooq, and B. Ratra, Phys. Rev. D **90**, 023006 (2014), 1312.5285.

[29] A. Gómez-Valent, J. Solà, and S. Basilakos, J. Cosmology Astropart. Phys. **1**, 004 (2015), 1409.7048.

[30] E. J. Ruiz and D. Huterer, Phys. Rev. D **91**, 063009 (2015), 1410.5832.

[31] E.-M. Mueller, W. Percival, E. Linder, S. Alam, G.-B. Zhao, A. G. Sánchez, F. Beutler, and J. Brinkmann, MNRAS **475**, 2122 (2018), 1612.00812.

[32] S. Nesseris, G. Pantazis, and L. Perivolaropoulos, Phys. Rev. D **96**, 023542 (2017), 1703.10538.

[33] J. Solà, A. Gómez-Valent, and J. de Cruz Pérez, Modern Physics Letters A **32**, 1750054-144 (2017), 1610.08965.

[34] L. Kazantzidis and L. Perivolaropoulos, ArXiv e-prints (2018), 1803.01337.

[35] O. Lahav, P. B. Lilje, J. R. Primack, and M. J. Rees, MNRAS **251**, 128 (1991).

[36] L. Wang and P. J. Steinhardt, ApJ **508**, 483 (1998), astro-ph/9804015.

[37] E. V. Linder, Phys. Rev. D **72**, 043529 (2005), astro-ph/0507263.

[38] B. L'Huillier, A. Shafieloo, and H. Kim, MNRAS **476**, 3263 (2018), 1712.04865.

[39] D. Polarski, A. A. Starobinsky, and H. Giacomini, J. Cosmology Astropart. Phys. **12**, 037 (2016), 1610.00363.

[40] D. Polarski and R. Gannouji, Physics Letters B **660**, 439 (2008), 0710.1510.

[41] R. Gannouji, B. Moraes, and D. Polarski, J. Cosmology Astropart. Phys. **2**, 034 (2009), 0809.3374.

[42] H. Motohashi, A. A. Starobinsky, and J. Yokoyama, Progress of Theoretical Physics **123**, 887 (2010), 1002.1141.

[43] C. Blake, S. Brough, M. Colless, C. Contreras, W. Couch, S. Croom, T. Davis, M. J. Drinkwater, K. Forster, D. Gilbank, et al., MNRAS **415**, 2876 (2011), 1104.2948.

[44] F. Beutler, C. Blake, M. Colless, D. H. Jones, L. Staveley-Smith, G. B. Poole, L. Campbell, Q. Parker, W. Saunders, and F. Watson, MNRAS **423**, 3430 (2012), 1204.4725.

[45] S. de la Torre and J. A. Peacock, MNRAS **435**, 743 (2013), 1212.3615.

[46] C. Howlett, A. J. Ross, L. Samushia, W. J. Percival, and M. Manera, MNRAS **449**, 848 (2015), 1409.3238.

[47] C. Howlett, L. Staveley-Smith, P. J. Elahi, T. Hong, T. H. Jarrett, D. H. Jones, B. S. Koribalski, L. M. Macri, K. L. Masters, and C. M. Springob, MNRAS **471**, 3135 (2017), 1706.05130.

[48] H. Gil-Marín, W. J. Percival, L. Verde, J. R. Brownstein, C.-H. Chuang, F.-S. Kitaura, S. A. Rodríguez-Torres, and M. D. Olmstead, MNRAS **465**, 1757 (2017), 1606.00439.

[49] T. Okumura, C. Hikage, T. Totani, M. Tonegawa, H. Okada, K. Glazebrook, C. Blake, P. G. Ferreira, S. More, A. Taruya, et al., PASJ **68**, 38 (2016), 1511.08083.

[50] S. Alam, S. Ho, and A. Silvestri, MNRAS **456**, 3743 (2016), 1509.05034.

[51] DESI Collaboration, A. Aghamousa, J. Aguilar, S. Ahlen, S. Alam, L. E. Allen, C. Allende Prieto, J. Annis, S. Bailey, C. Balland, et al., ArXiv e-prints (2016), 1611.00036.

[52] DESI Collaboration, A. Aghamousa, J. Aguilar, S. Ahlen, S. Alam, L. E. Allen, C. Allende Prieto, J. Annis, S. Bailey, C. Balland, et al., ArXiv e-prints (2016), 1611.00037.

[53] Z. Ivezic, J. A. Tyson, B. Abel, E. Acosta, R. Allsman, Y. AlSayyad, S. F. Anderson, J. Andrew, R. Angel, G. Angeli, et al., ArXiv e-prints (2008), 0805.2366.